JOURNAL OF GUIDANCE, CONTROL, AND DYNAMICS
Vol. 34, No. 4, July–August 2011

High-Accuracy Trajectory Optimization for a Trans-Earth Lunar Mission

Hui Yan* and Qi Gong†
University of California, Santa Cruz, California 95064
Chan D. Park‡ and I. Michael Ross§
U.S. Naval Postgraduate School, Monterey, California 93943
and
Christopher N. D'Souza¶
NASA Johnson Space Center, Houston, Texas 77058

DOI: 10.2514/1.49237

The trajectory optimization of a spacecraft subject to the gravitational effects of the moon, Earth, and sun are considered. The problem is how to achieve Earth-interface conditions from a low lunar orbit. Practical constraints of maximum thrust, fuel budget, and flight time generates a constrained, nonautonomous, nonlinear optimal control problem. Severe constraints on the fuel budget combined with high-accuracy demands on the endpoint conditions necessitate a high-accuracy solution to the trajectory optimization problem. The problem is first solved using the standard Legendre pseudospectral method. The optimality of the solution is verified by an application of the covector mapping principle. It is shown that the thrust structure consists of three finite burns with nearly linear steering-angle time histories. A singular arc is detected and is interpreted as a singular plane change maneuver. The Bellman pseudospectral method is then employed for mesh refinement to improve the accuracy of the solution.

I. Introduction

A KEY challenge in interplanetary trajectory optimization is the long-time propagation sensitivity of the optimal solution. Miele and Wang [1] note that a small error in the launch velocity at low Earth orbit can induce a very large position error at Mars arrival due to the long-flight-time propagation of various errors. This sensitivity generates a special challenge in the design of a guidance, navigation, and control (GNC) system. The challenge is typically met by budgeting errors on the various subsystems that comprise the overall GNC system. In this regard, consider a trajectory accuracy requirement of a 1 km ball before an escape from a lunar orbit in a moon-Earth mission. We generate an optimal trajectory with the boundary conditions and spacecraft parameters defined in [2], and suppose the optimal thrust direction and magnitude at a low lunar orbit (LLO) is perturbed by just 0.01%, which is equivalent to a velocity error of only 1.55 m/s; then, as shown in Fig. 1, the final position error is 313 km, well-outside the 1 km requirement. Additional details on the moon-Earth trajectory dispersion analysis are given by D'Souza et al. [3].

In this paper, we propose a numerical technique to design fuel-optimal trajectories that meet a position error requirement of less than 1 km. One might ask the question: why is such accuracy needed for trajectory propagation? The answer to this question lies is engineering systems' analysis. In system design, a designer needs to understand the sensitivities of the guidance, control and navigation subsystems separately and independently. These sensitivities are used to establish error budgets for propellant and, thereby, vehicle sizing for weight, power, and volume. The error budgets allow the system designer the appropriate decision variables to perform tradeoffs and expose those variables for which a higher return (e.g., mass margin) can be achieved with minimal investment (e.g., algorithm complexity and performance). Furthermore, error margins can be traded between guidance/targeting, navigation, and control to find the "best solution" from a systems' perspective. In an early design phase, mass is the "coin of the realm," whereas in the later phases, it is software complexity. Thus, the ideal targeting algorithm is the one that is highly accurate (in the sense of optimality, and hence achieving the most mass margin) with least computational burden (software complexity). Therefore, in the design process, it is necessary to obtain the sensitivities of the guidance/targeting, navigation and control subsystems with respect to the parameters of interest (mass or software complexity, however, that is defined) and thus establish the foundation for an "optimal" design subject to the various systems' constraints.

Human spaceflight places yet another challenge on the design of a GNC system. The imposition of "Anytime Return" along with limited onboard fuel implies very tight margins with guaranteed performance. Past techniques to meet these challenges have resulted in high costs in terms of extensive planning and limited flexibility in mission changes. For instance, in the 1960s, this problem was solved through a series of approximations [4–6] that were eventually compensated by higher onboard fuel for corrections. As cost reduction is the key to a realizing a modern human spaceflight, a new question that has come about as a result of the Constellation program [7] is a means to streamline the process of trajectory optimization.

In response to these new challenges, finite-burn techniques have been developed [8,9] under an assumption of constant thrust and steering rates to optimize escape trajectories that build upon impulsive maneuver models. Weeks et al. [2] and Scarritt et al. [10] propose an onboard autonomous targeting algorithm for the moon-Earth transfer, based on a linear two-level corrections process. In their work, the magnitude of thrust is also assumed constant and the thrust steering rate is constant or zero. In this paper, we develop a high-accuracy trajectory optimization technique for a trans-Earth mission with significant orbit plane change that is specifically designed for future manned lunar missions [7]. Recognizing that both the time of flight and fuel consumption are critical factors for manned missions, we aim to develop a readily implementable control strategy that

Received 5 February 2010; revision received 7 January 2011; accepted for publication 8 January 2011.

*Research Associate, Dept. of Applied Mathematics and Statistics.
†Assistant Professor, Dept. of Applied Mathematics and Statistics.
‡Research Associate, Dept. of Mechanical and Aerospace Engineering.
§Professor, Dept. of Mechanical and Aerospace Engineering.
¶Orion Navigation Subsystem Manager, Orion Relative Navigation Lead, EG6, Aerosciences and Flight Mechanics Division.

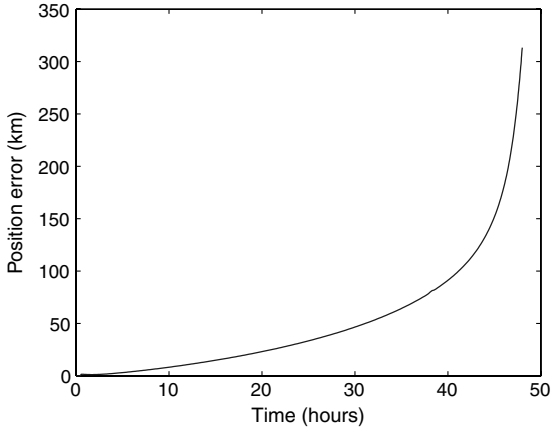

Fig. 1 Illustrating the high sensitivity of a fuel-optimal moon-Earth trajectory.

minimizes fuel consumption under practical and operational flight constraints. More specifically, we directly design a sequence of *finite* burn maneuvers that transfers the spacecraft from a low lunar parking orbit to a specified position and velocity vector that is designed to target a specific Earth interface condition.

The trajectory design is formulated as a constrained nonlinear optimal control problem. The thrust and the steering angle rate are allowed to vary. No assumptions are made on the control switching structure or on steering rates. To this end, the dynamics is represented in a moon-centered *translating* (but not rotating) Cartesian coordinate frame aligned with the J2000 inertial frame. Orbital motions of the sun and the Earth with respect to the moon are taken from actual ephemerides data. Based on these equations of motion and other design requirements, we formulate a time-bounded fuel-optimal control problem, which is nonlinear and nonautonomous (i.e., time varying). To solve the resulting optimal control problem, we adopt the Legendre pseudospectral (PS) method implemented in DIDO© [11]. Over the last decade, PS methods for optimal control have moved rapidly from theory to flight applications [12–15], the most famous of this being the discovery and implementation of the "zero-propellant maneuver" onboard the International Space Station [12,13]. Thanks to the popularity of software packages such as OTIS [16] and DIDO©, PS methods are used quite routinely within the aerospace community. In this paper, we use PS methods to solve the moon-Earth transfer problem to a very high accuracy. The high accuracy comes from two aspects: one from the high fidelity of the dynamical model and the other from the precise computation of the control trajectory.

II. Problem Formulation

A. Equations of Motion

We formulate the equations of motion in the J2000 moon-centered *translating* Mxyz Cartesian frame. The origin of the J2000 moon-centered frame is attached to and moves with the moon, but the axis orientations are aligned with the direction of the J2000 sun-centered frame. We assume the J2000 sun-centered frame is inertial. The J2000 sun-centered inertial Cartesian Frame *SXYZ* is defined as follows: The reference epoch is set at the J2000 epoch. The *XY* plane is the plane of Earth's orbit at the reference epoch. The *X* axis points to the ascending node of the instantaneous plane of Earth's orbit and Earth's mean equator at the reference epoch. The *Z* axis is perpendicular to the *XY* plane in the directional sense of Earth's north pole at the reference epoch. The *Y* axis is determined by the right-hand rule.

We select Cartesian coordinates to solve the problem rather than spherical coordinates. This choice of coordinates allows us to avoid the singularity in spherical coordinates which occurs when the trajectory crosses the z axis so that we may freely allow the return trajectory to be in any plane. The equations of motion are as follows [17]:

$$\dot{x} = v_x \qquad \dot{y} = v_y \qquad \dot{z} = v_z$$

$$\dot{v}_x = -\frac{\mu_M x}{r_M^3} - \frac{\mu_E(x - x_E)}{r_E^3} - \frac{\mu_S(x - x_S)}{r_S^3} + \frac{T\cos\alpha\cos\beta}{m} - \ddot{x}_M(t)$$

$$\dot{v}_y = -\frac{\mu_M y}{r_M^3} - \frac{\mu_E(y - y_E)}{r_E^3} - \frac{\mu_S(y - y_S)}{r_S^3} + \frac{T\sin\alpha\cos\beta}{m} - \ddot{y}_M(t)$$

$$\dot{v}_z = -\frac{\mu_M z}{r_M^3} - \frac{\mu_E(z - z_E)}{r_E^3} - \frac{\mu_S(z - z_S)}{r_S^3} + \frac{T\sin\beta}{m} - \ddot{z}_M(t)$$

$$\dot{m} = -\frac{T}{v_e} \tag{1}$$

Here (x, y, z) and (v_x, v_y, v_z) are the spacecraft positions and velocities along the moon-centered frame, respectively. m is the mass of the spacecraft. T is the thrust of the spacecraft, and $\beta \in [-\pi/2, +\pi/2]$ and $\alpha \in [0, 2\pi]$ are the elevation and azimuth of the thrust vector defined in spherical coordinates. $(\ddot{x}_M(t), \ddot{y}_M(t), \ddot{z}_M(t))$ are, respectively, the moon's translating acceleration components along the moon-centered frame; (μ_M, μ_E, μ_S) are the gravitational constants of the moon, Earth, and sun, respectively, v_e is the characteristic exhaust velocity, (x_E, y_E, z_E) and (x_S, y_S, z_S) are, respectively, the time-varying position components of the Earth and the sun with respect to the instantaneous center of the moon, and (r_M, r_E, r_S) are the distances of the spacecraft from the moon, the Earth, and the sun, respectively.

B. Ephemerides

The relative motions of the Earth and the sun with respect to the moon are incorporated by their respective ephemerides data obtained from the Jet Propulsion Laboratory's HORIZONS website.** For the ephemerides, $t \mapsto (x_E, y_E, z_E)$ and $t \mapsto (x_S, y_S, z_S)$, we first import sampled data from HORIZONS in 1-min intervals for a given operational time span between 2 April 2024 and 12 April 2024. Then, we conduct a polynomial interpolation to redefine those data as functions of time. For the lunar acceleration $\ddot{\boldsymbol{r}}_{M/S} = [\ddot{x}_M \quad \ddot{y}_M \quad \ddot{z}_M]^T$, we import the sampled lunar velocity in the inertial frame from HORIZONS, derive it as a function of time using polynomial interpolation, and then differentiate the polynomial with respect to time. A $n = 12$ deg polynomial approximation is used for evaluating $(x_E, y_E, z_E)(t)$, $(x_S, y_S, z_S)(t)$, and $(\ddot{x}_M, \ddot{y}_M, \ddot{z}_M)(t)$. The coefficients of these polynomials for the three components of the sun and Earth position are shown in Table 1. Thus, for any time t, the position of the sun and Earth with respect to the moon can be quickly obtained from

$$P = \sum_{k=0}^{n} a_k t^{n-k} \tag{2}$$

where P applies to either the sun or Earth's position with the appropriate coefficients. As shown in Figs. 2 and 3 this approach is quite accurate: the position errors between the ephemerides and interpolation is at an order of 10^{-3} km for both sun and Earth.

C. Boundary Conditions

We choose the boundary conditions studied in [2,10,18]. The initial epoch is given as 4 April 2024 15:30:00TDT. The initial condition is given in the J2000 moon-centered frame and represents a 100 km-altitude corresponding to a low lunar circular orbit

$$\begin{bmatrix} x(t_0) \\ y(t_0) \\ z(t_0) \\ v_x(t_0) \\ v_y(t_0) \\ v_z(t_0) \end{bmatrix} = \begin{bmatrix} -1.2367970783385588 \times 10^3 \text{ km} \\ 1.2681142350088496 \times 10^3 \text{ km} \\ 4.6838317094160635 \times 10^2 \text{ km} \\ 3.291108058365355 \times 10^{-2} \text{ km/ sec} \\ 5.89269803607714 \times 10^{-1} \text{ km/ sec} \\ -1.528058717568413 \times 10^0 \text{ km/ sec} \end{bmatrix} \tag{3}$$

**Additional data available on HORIZONS SYSTEM available at http://ssd.jpl.nasa.gov/?horizons [accessed May 2009].

Table 1 Coefficients of the polynomial function in Eq. (2)

a_k	Coef. of x_S	Coef. of y_S	Coef. of z_S	Coef. of x_E	Coef. of y_E	Coef. of z_E
a_0	−1.1900e − 7	5.1363e − 8	3.1236e − 8	−1.2047e − 7	5.2002e − 8	3.1623e − 8
a_1	7.5355e − 6	−1.8138e − 6	−1.1952e − 6	7.6284e − 6	−1.8365e − 6	−1.2101e − 6
a_2	−1.9394e − 4	8.6037e − 6	1.0045e − 5	−1.9633e − 4	8.7190e − 6	1.0172e − 5
a_3	2.5517e − 3	4.1141e − 4	1.5326e − 4	2.5831e − 3	4.1634e − 4	1.5509e − 4
a_4	−1.8494e − 2	−6.2236e − 3	−2.8743e − 3	−1.8723e − 2	−6.2990e − 3	−2.9092e − 3
a_5	9.6451e − 2	2.9032e − 2	1.3126e − 2	9.7640e − 2	2.9382e − 2	1.3285e − 2
a_6	−4.8792e − 1	−2.4592e − 1	−1.2033e − 1	−4.9393e − 1	−2.4891e − 1	−1.2180e − 1
a_7	−1.8082e0	1.4769e0	8.5354e − 1	−1.8295e0	1.4934e0	8.6331e − 1
a_8	−2.6567e − 1	4.5036e1	2.4513e1	−7.9456e − 1	4.5426e1	2.4744e1
a_9	8.4469e2	5.8795e1	2.1895e1	8.2187e2	1.7358e2	7.1608e1
a_{10}	−1.8090e4	−1.3292e4	−6.8199e3	3.5271e3	−8.8123e3	−4.8913e3
a_{11}	−6.2097e5	2.2783e6	9.8643e5	−8.2856e4	−3.1492e4	−1.4835e4
a_{12}	1.4557e8	3.1280e7	1.3596e7	−1.2500e5	3.1052e5	1.7237e5

The terminal condition is given by

$$\begin{bmatrix} x(t_f) \\ y(t_f) \\ z(t_f) \\ v_x(t_f) \\ v_y(t_f) \\ v_z(t_f) \end{bmatrix} = \begin{bmatrix} 2.10640349727063 \times 10^3 \text{ km} \\ 3.59640440859595 \times 10^3 \text{ km} \\ 6.08167937792834 \times 10^2 \text{ km} \\ -1.51018343429892 \times 10^{-1} \text{ km/s} \\ -3.21178999121464 \times 10^{-1} \text{ km/s} \\ -1.79844521633271 \times 10^0 \text{ km/s} \end{bmatrix} \tag{4}$$

D. Spacecraft Specification and Other Design Requirements

The rocket we consider in this paper has the following specification [2,10,18]:

1) Total mass is $m_0 = 20,\ 339.9$ kg and specific impulse is $I_{\text{sp}} = 326$ s.

2) Maximum engine thrust is $T_{\max} = 33.3616621$ kN and maximum allowable fuel is $m_{\text{fuel}} = 8,063.65$ kg.

3) Flight time $t_f - t_0 \leq 2$ days.

E. Finite-Thrust Fuel-Optimal Control Problem

Taking into account the previously derived equations of motion and various constraints, we now formulate a finite-thrust time-bounded fuel-optimal control problem for designing trans-Earth trajectories from the moon.

Problem 1: Find the thrust vector time history to minimize the fuel consumption

$$J = m_0 - m_f$$

subject to the four-body dynamic equations of motion (1). The initial epoch t_0 is 4 April 2024 15:30 : 00TDT and the transfer time is constrained by $t_f - t_0 \leq 2$ days. The initial conditions are given by Eq. (3) along with $m_0 = 20,339.9$ kg, and the terminal conditions are given by Eq. (4). The finite-thrust magnitude is bounded by

$$0 \leq T \leq T_{\max} = 33.3616621 \text{ kN}$$

Remark 1: In the aforementioned trajectory optimization problem, we address the full minimum fuel control problem in one step. The dynamics directly incorporate multibody effects. There are no impulsive approximations with no preassumed burn structure. The solution to the formulated optimal control problem will provide a fuel-optimal finite-burn trajectory.

As explained in the introduction section, the combined effects of the high-accuracy requirement, the use of high-fidelity models, and the long-time span make the problem extremely sensitive to the control profile. To achieve the design requirements including fuel optimality and high accuracy, an efficient trajectory optimization tool has to be used. A proper pseudospectral method meets these requirements.

III. Short Introduction to Pseudospectral Methods

Based on their orthogonal properties, PS methods come in different flavors such as Legendre and Chebyhsev methods [19–25]. The methods of choice for optimal control problems are Legendre PS methods because the orthogonality of the Legendre polynomials with respect to a unit weight function avoids much of the clutter associated with nonunit weight functions [22,23]. Among the various choices of node points, we select the one based on Gauss–Lobatto points as the choices of other points are inappropriate [22,23,26] for standard optimal control problems. As summarized in Fig. 4, a choice of uniform points offers the worst performance, while Gauss–Lobatto points offer the best performance, and everything else is in the middle to varying degrees of applicability [27]. Thus, it is possible to inadvertently design a bad pseudospectral method [26].

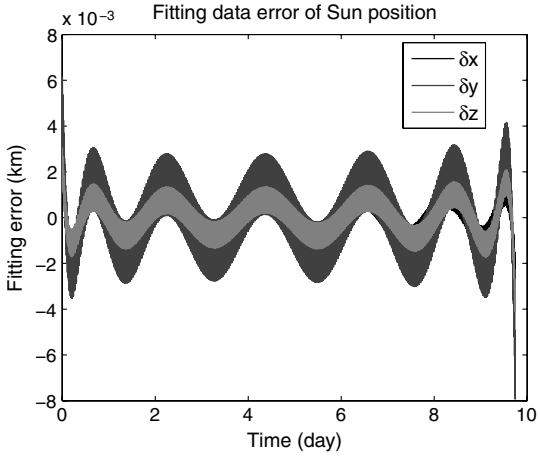

Fig. 2 Curve-fitting errors for sun's position.

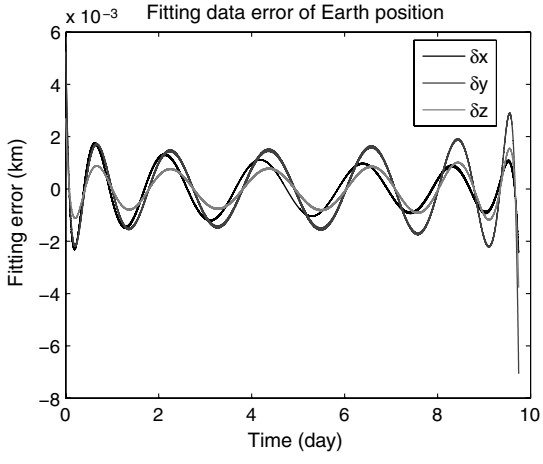

Fig. 3 Fitting error of Earth position.

Increasing Generality →

Decreasing Applicability ↓

	Free Endpoints	One Endpoint Fixed	Arbitrary Endpoints
Gauss-Lobatto	Yes	Yes	Yes
Gauss-Radau	Yes	Yes	No
Gauss	Yes	No	No
Uniform	No	No	No

Fig. 4 Applicability of node points for pseudospectral optimal control; from [27].

Among all possible node points for discretizing optimal control, the Gauss–Lobatto points are the only set of grid points for which feasibility, consistency, and convergence of the approximations can be mathematically guaranteed [28–30]. While other node points are useful in other fields, only the Gauss–Lobatto points are useful for finite-horizon optimal control. Because of their fast convergence rates, we expect PS methods to have a lower computational burden than other methods particularly since the flight time from moon to Earth usually takes several days resulting in a need for a very fine mesh to generate an accurate solution.

Suppose we consider a general optimal control problem of the following form:

Problem B: Determine the state-control function pair $t \mapsto (\boldsymbol{x}, \boldsymbol{u}) \in \mathbb{R}^{N_x} \times \mathbb{R}^{N_u}$ and initial/final time $(t_0,\ t_f)$ that minimize the cost functional

$$J[\boldsymbol{x}(\cdot), \boldsymbol{u}(\cdot), t_0, t_f] = E(\boldsymbol{x}(t_0), \boldsymbol{x}(t_f), t_0, t_f) + \int_{t_0}^{t_f} F(\boldsymbol{x}(t), \boldsymbol{u}(t))\, \mathrm{d}t$$

subject to dynamics

$$\frac{\mathrm{d}\boldsymbol{x}}{\mathrm{d}t} = \boldsymbol{f}(\boldsymbol{x}, \boldsymbol{u}, t)$$

boundary conditions $\boldsymbol{e}(\boldsymbol{x}(t_0), \boldsymbol{x}(t_f), t_0, t_f) = \boldsymbol{0}$, control constraints $\boldsymbol{u}_{\min} \le \boldsymbol{u} \le \boldsymbol{u}_{\max}$, and path constraints $\boldsymbol{h}(\boldsymbol{x}, t) \le \boldsymbol{0}$.

For notation simplicity, we consider only time-invariant systems in Problem B. Any time-varying system can easily be transferred to time-invariant one by augmenting time t into state variable. The core idea of any PS method for optimal control is to use Lagrange polynomials to globally interpolate the state at the appropriate Gauss–Lobatto points. Then, through discretization, the optimal control problem is solved by a spectral algorithm [25,31]. In the Legendre PS method, the trajectory $\boldsymbol{x}(t)$ is approximated by N-th order polynomials $\boldsymbol{x}^N(t)$ based on the interpolation at the shifted Legendre–Gauss–Lobatto (LGL) quadrature nodes:

$$\boldsymbol{x}(t) \approx \boldsymbol{x}^N(t) = \sum_{k=0}^{N} \boldsymbol{x}^N(t_k)\phi_k(t)$$

Here $t_k = \frac{t_f - t_0}{2}(\tau_k + 1), k = 0, \cdots, N$ are the shifted LGL nodes, and $\tau_k = -1, \cdots, 1,\ k = 0, \cdots, N$ are the roots of the derivative of the N-th order Legendre polynomial. $\phi_k(t)$ are the Lagrange interpolating polynomial.

The derivative of the i-th state $x_i(t)$ at the LGL node t_k can be approximated by

$$\dot{x}_i(t_k) \approx \dot{x}_i^N(t_k) = \sum_{j=0}^{N} D_{kj} x_i^N(t_j), \qquad i = 1, 2, \cdots, N_x$$

where $(N+1) \times (N+1)$ differentiation matrix D is defined as

$$D_{ik} = \frac{2}{t_f - t_0} \begin{cases} \frac{L_N(\tau_i)}{L_N(\tau_k)} \frac{1}{\tau_i - \tau_k}, & \text{if } i \ne k; \\ -\frac{N(N+1)}{4}, & \text{if } i = k = 0; \\ \frac{N(N+1)}{4}, & \text{if } i = k = N; \\ 0, & \text{otherwise} \end{cases}$$

Let $\bar{x}_k = x^N(t_k),\ k = 0, 1, \cdots, N$. The differential equation is approximated by the following nonlinear algebraic inequalities

$$\left\| \sum_{i=0}^{N} \bar{x}_i D_{ki} - f(\bar{\boldsymbol{x}}_k, \bar{\boldsymbol{u}}_k, t_k) \right\|_\infty \le \delta \tag{5}$$

where $\delta > 0$ is a small number representing the feasibility tolerance. The notation $\bar{(\cdot)}$ is used to denote discretized variables. Note that the subscript in $\bar{\boldsymbol{x}}_k$ denotes an evaluation of the approximate state $\boldsymbol{x}^N(t) \in \mathbb{R}^{N_x}$ at the node t_k, whereas $x_k(t)$ denotes the k-th component of the exact state. The endpoint conditions and constraints are approximated in a similar fashion:

$$\begin{aligned} &\|\boldsymbol{e}(\bar{x}_0, \bar{x}_N, t_0, t_N)\|_\infty \le \delta \qquad \boldsymbol{h}(\bar{\boldsymbol{x}}_k, t_k) \le \delta \cdot \boldsymbol{1}, \\ &k = 0, \cdots, N, \qquad \boldsymbol{1} = [1, \cdots, 1]^T \end{aligned} \tag{6}$$

Finally, the cost functional $J[\boldsymbol{x}(\cdot), \boldsymbol{u}(\cdot), t_0, t_f]$ is approximated by the Gauss–Lobatto integration rule:

$$\begin{aligned} J[\boldsymbol{x}(\cdot), \boldsymbol{u}(\cdot), t_0, t_f] \approx \bar{J}^N = \frac{t_N - t_0}{2} \sum_{k=0}^{N} F(\bar{\boldsymbol{x}}_k, \bar{\boldsymbol{u}}_k, t_k) w_k \\ + E(\bar{\boldsymbol{x}}_0, \bar{\boldsymbol{x}}_N, t_0, t_N) \end{aligned} \tag{7}$$

where

$$w_k = \frac{2}{N(N+1)} \frac{1}{[L_N(\tau_k)]^2}$$

Thus, the optimal control Problem B is approximated by the discretized problem:

Problem B^N: Find $\bar{\boldsymbol{x}}_k \in \mathbf{X},\ \bar{\boldsymbol{u}}_k \in \mathbf{U},\ k = 0, 1, \cdots, N$, and t_0, $t_N \in \mathbf{T}$ that minimize the cost function (7), subject to constraints (5) and (6).

The theoretical analysis in Gong et al. [28] shows the well-posedness of PS discretization, which preserves the feasibility of the original continuous Problem B and is a consistent approximation in the sense of Polak [32].

IV. Optimality Conditions

Since the fuel optimality is the most important requirement of the design, it is necessary to verify the optimality of the computed solution. This is done via the covector mapping principle [27,29]. As illustrated in Fig. 5, although there are no continuous adjoint equations directly involved in the discretization, the continuous costate information can still be obtained through an application of the covector mapping principle. The covectors can then be used for optimality verification by an application of Pontryagin's principle [33].

In this section, we derive some necessary conditions that will be used later for verification purposes. The necessary conditions to minimize J can be obtained from minimizing the Hamiltonian H given by

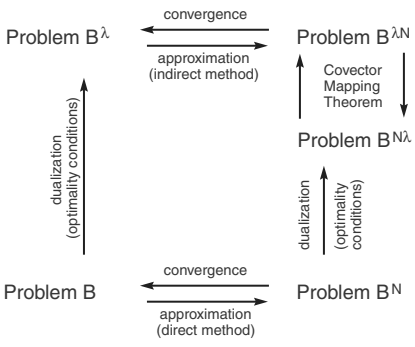

Fig. 5 Illustrating the covector mapping principle and the covector mapping theorem [27,29].

$$H = \boldsymbol{\lambda}_r^T \boldsymbol{v} + \boldsymbol{\lambda}_v^T \boldsymbol{g}(\boldsymbol{r}) + \frac{\boldsymbol{\lambda}_v^T \boldsymbol{T}}{m} - \frac{\lambda_m T}{v_e} \tag{8}$$

where

$$\boldsymbol{g}(\boldsymbol{r}) = -\frac{\mu_M}{r_M^3}\boldsymbol{r}_M - \frac{\mu_E}{r_E^3}\boldsymbol{r}_E - \frac{\mu_S}{r_S^3}\boldsymbol{r}_S - \ddot{\boldsymbol{r}}_{M/S}(t)$$

$\boldsymbol{\lambda}_r$, $\boldsymbol{\lambda}_v$, and λ_m represent the position, velocity, and mass costates, respectively. $\boldsymbol{T}$ stands for the thrust vector, and $\boldsymbol{r_M}$, $\boldsymbol{r_E}$, and $\boldsymbol{r_S}$ are the spacecraft position vectors from the moon, the Earth, and the sun, respectively. The adjoint equations are

$$\dot{\boldsymbol{\lambda}}_r = -\left(\frac{\partial \boldsymbol{g}}{\partial \boldsymbol{r}}\right)^T \boldsymbol{\lambda}_v \qquad \dot{\boldsymbol{\lambda}}_v = -\boldsymbol{\lambda}_r \qquad \dot{\lambda}_m = \frac{-\lambda_v T}{m^2} \tag{9}$$

From the Hamiltonian minimization condition [33], the following necessary conditions hold

$$\frac{\boldsymbol{T}}{T} = \frac{-\boldsymbol{\lambda}_v}{\lambda_v} \qquad T = \begin{cases} 0, & \text{when } S > 0 \\ T_{\max} & \text{when } S < 0 \\ \text{Singular} & \text{when } S \equiv 0 \end{cases} \tag{10}$$

$$\lambda_m(t_f) = -1 \tag{11}$$

where $S = -\frac{\lambda_v}{m} - \frac{\lambda_m}{v_e}$ is a switching function and $\lambda_v = \|\boldsymbol{\lambda}_v\|$.

V. Solution by Standard Pseudospectral Methods

Scaling is one of the most important techniques for a successful computation. For the problem at hand, we choose canonical moon units to scale the dynamics. All numerical optimizations for solving the problem were performed using DIDO©, a MATLAB® package for solving optimal control problems using PS methods [11]. Once we provide such essential data as the system dynamics, boundary conditions, control bounds, path constraints, etc, in its original form, DIDO implements a version of the spectral algorithm [31] to generate a candidate optimal trajectory and control. DIDO also generates the costates and Hamiltonian trajectory by way of the covector mapping theorem [28]. This feature of PS methods provides an easy way to verify and validate the computed solution by applying Pontryagin's principle. Additional details on how to use DIDO are provided in [11].

A. Results from Standard Pseudospectral methods

Figures 6–8 show the optimal solution by standard Legendre PS methods with 300 LGL points. The thrust profile is shown in Fig. 6. It clearly demonstrates three finite burns separated by coast arcs. Note that we never enforce a three burn structure in our problem setting.

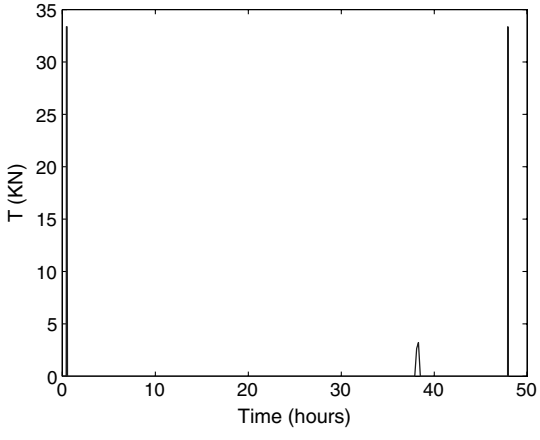

Fig. 6 Thrust control structure.

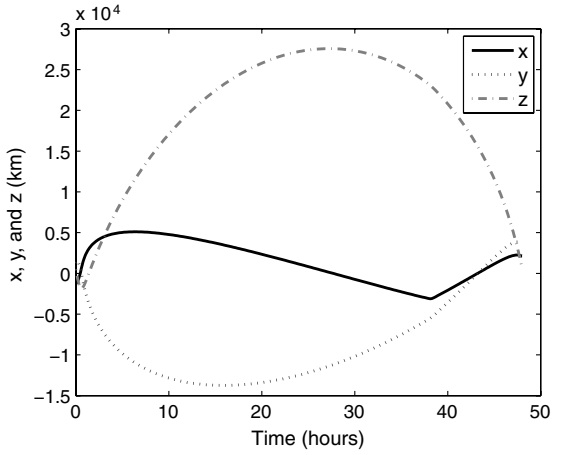

Fig. 7 Position.

DIDO's spectral algorithm automatically discovered this structure. Note also that not all burns are bang–bang. The second burn appears to be a singular arc. A detailed analysis on the optimality of this singular arc is presented in [34,35]. To limit the scope of this paper, we present a "first-order" analysis on the optimality of the computed solution.

Figures 7 and 8 illustrate the position and velocity time histories. The final position and velocity errors are within $1e-10$ km and $1e-10$ km/s, respectively, which is much less than tolerance criterion. The flight time is 48 hours.

The fuel consumptions for the first, second, and third burn are 3538.5, 1333.5, and 1783.7 kg, respectively, with the total fuel consumption 6655.7 kg, and about a half of the fuel is used in the first burn.

B. Optimality Verification

To verify the optimality of the computed solution, we use the covector mapping principle to automatically compute all the costate information. Then, the necessary conditions derived in Sec. IV can easily be verified. First, as indicated in Eq. (10), the thrust steering vector must be in the opposite direction of the costate vector associated with the velocity. Shown in Fig. 9 is the angle between the velocity costate vector and the thrust steering vector. The plots clearly demonstrate that the two vectors are indeed in the inverse direction; this verifies the necessary condition (10). Figure 10 indicates the final transversality condition Eq. (11) is also satisfied. Since the optimal solution of this multibody problem includes a singular arc, the optimality verification of Eq. (11) is much more subtle and elaborate. We have carried out the optimality analysis on the singular arc in [34,35].

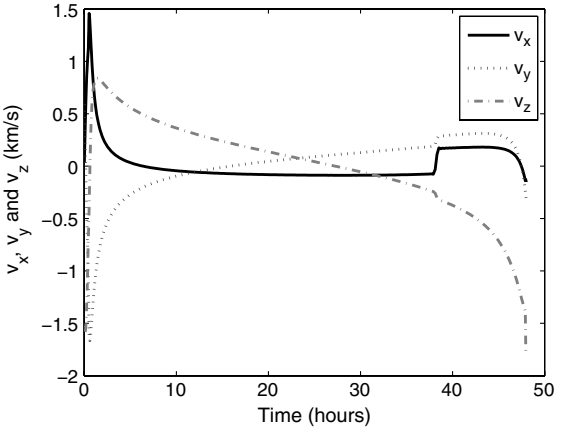

Fig. 8 Velocity.

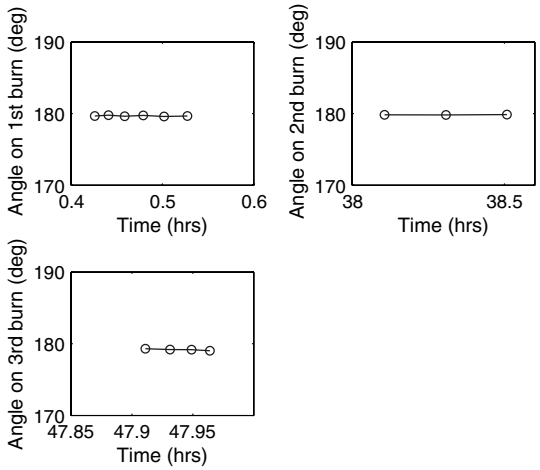

Fig. 9 Angle between the primer vector and thrust vector.

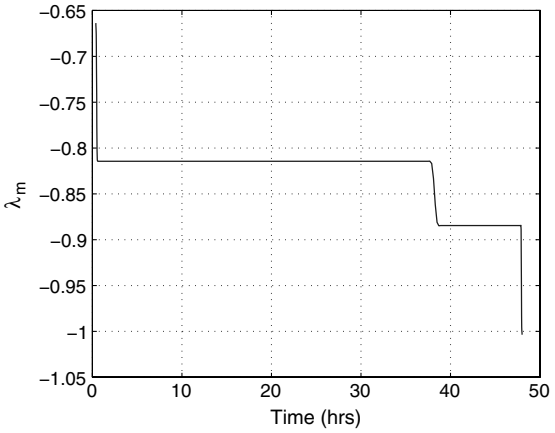

Fig. 10 Mass costate.

VI. Practical Implementation Considerations

Solutions from PS methods, or for that matter, any numerical method, are given in discrete time. For practical implementation, we need to map the discrete controls to implementable controls. For instance, a zero-order hold is an implementable control. To determine practical feasibility, we need to map a discrete-time controller to a continuous-time domain and examine the continuous-time feasibility of the resulting solution. The discrete-time to continuous-time mapping can be done using various interpolation methods. Once the continuous-time control profile is obtained, we can verify the feasibility of computed solution through a high-precision propagator. As noted in the introduction section, the problem is highly sensitive; hence, the slightest amount of interpolation error will be amplified causing large terminal errors. Indeed, a velocity difference of about 6×10^{-4} km/s at the beginning of transfer may cause final position errors of about 100 km after 48 hours of flight. Consequently, we first need to determine the appropriate method for interpolating the control signals and its impact on targeting errors.

A. Effects of Control Implementation

Consider first the nearest-neighbor interpolation. The interpolated thrust values are shown in Fig. 11. The final position and velocity errors are 644 km and 0.12 km/s, respectively, indicating the high sensitivity of the propagation. Note that, the discrete-time trajectory from PS methods has a final position and velocity errors within $1e-10$ km and $1e-10$ km/s, respectively. The discrepancy between discrete-time and continuous-time feasibility is due to the interpolation that maps the discrete control to the continuous one.

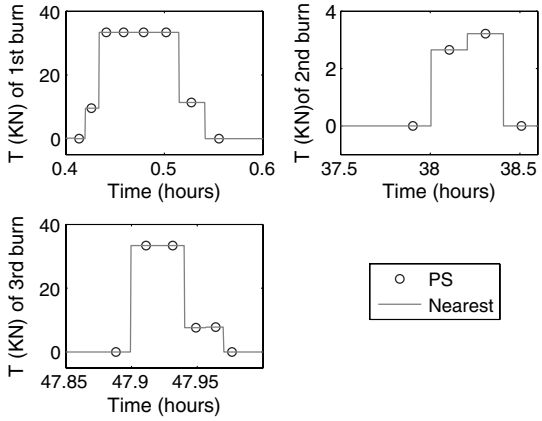

Fig. 11 Nearest neighbor interpolation.

Next, we examine the effects of two other control interpolations: linear and piecewise-cubic-Hermite. All of these interpolation techniques are readily available in MATLAB. The results are summarized in Table 2. It is clear from this table that our numerical experiment demonstrates the high sensitivity of the terminal error to various control interpolations.

To achieve the desired accuracy practically, we need to reduce the interpolation errors so that the continuous control profile can be accurately captured by the discrete one. We also need to prevent the amplification of the interpolation error through long-time span propagation. A brute-force approach is to increase the discretization points; i.e., refine the mesh. Because the control profile is expected to be composed of isolated narrow finite burns separated by dominant coast regions, a brute-force mesh refinement technique would be numerically inefficient [36,37]. This is because a mesh-refinement technique must not only account for the accuracy of the solution but also for obtaining higher resolution of the control signal leading to an inefficient computation due to the consequence of aliasing [36]. As a means to balance these competing interests, we explore the Bellman PS method as an efficient, targeted mesh refinement technique for reducing the interpolation and propagation errors. Since the errors from the "nearest" method are much less than ones from "pchip" and "linear," we will use the nearest method as the preferred choice of interpolation for the remaining part of this paper.

B. Bellman Pseudospectral Method

In the Bellman PS method [36], high-resolution solutions are sought merely near the initial conditions whereas the full solution is sequentially obtained by moving the initial conditions toward the final conditions by an application of Bellman's principle of optimality. The basic idea of the Bellman technique is illustrated in Fig. 12 and summarized in the following algorithm:

1) Solve the optimization problem for a reasonably low number of nodes n. This generates a discrete time solution $(\boldsymbol{x}_i, \boldsymbol{u}_i)$, $i = 0, \cdots, n$.

2) Partition the time interval $[t_0, t_n]$ into N_B Bellman segments $t^0 < t^1 < \cdots < t^{N_B} = t^n$, which are not necessarily uniformly spaced.

3) Propagate the system dynamics from t^0 to t^1 using $\boldsymbol{x}_0$ as the initial condition and any method of continuous-time reconstruction of the controls, $\boldsymbol{u}^1(t)$, $t \in [t^0, t^1]$.

4) Set $\boldsymbol{x}_0 = \boldsymbol{x}^1(t^1)$ and $t^0 = t^1$ and go to Step 1.

Table 2 Effects of various interpolation schemes

	Final position error, km	Fuel consumption, kg	Flight time, hrs
PS methods	0	6655.7	48.00
Nearest	644.0	6656.1	48.00
Pchip	2575.2	6655.1	48.00
Linear	7599.7	6655.7	48.00

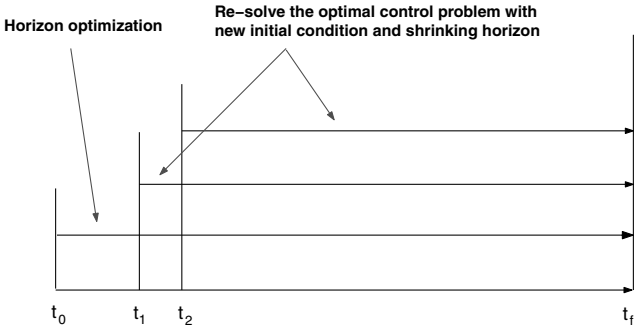

Fig. 12 Illustrating the Bellman PS technique.

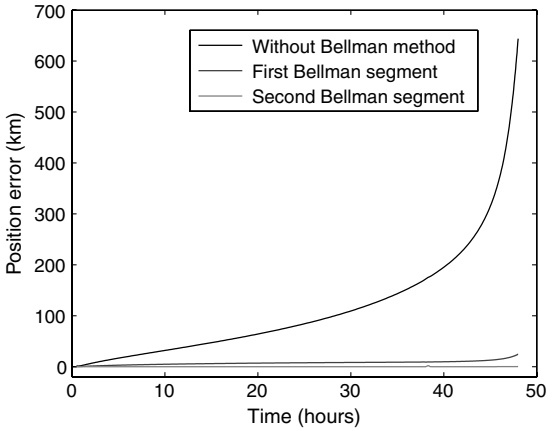

Fig. 13 Position error.

5) The algorithm stops at the N_B-th sequence when the final conditions are met. The candidate optimal trajectory and control is given by the Bellman chain:

$$\boldsymbol{x}^1(t), t \in [t^0, t^1]; \qquad \boldsymbol{x}^2(t), t \in [t^1, t^2]; \cdots, \boldsymbol{x}^{N_B}(t), t \in [t^{N_B-1}, t^{N_B}]$$

$$\boldsymbol{u}^1(t), t \in [t^0, t^1]; \qquad \boldsymbol{u}^2(t), t \in [t^1, t^2]; \cdots, \boldsymbol{u}^{N_B}(t), t \in [t^{N_B-1}, t^{N_B}]$$

When the Bellman technique is combined with the property of PS methods, it creates an efficient way for targeted mesh refinement and reduces interpolation errors. To see this, notice that the distribution of the LGL nodes is dense around the ends and sparse in the middle. This means that around the partition points, t^i, we will naturally get a dense distribution of the nodes. By tuning the partition points, we can distribute more nodes to the points where the control contains large variations. Therefore, the mapping from discrete-time control to the continuous-time one can be made more accurate around the points of interest. In this way, the interpolation error can be reduced. On the other hand, any propagation error that occurs before the new Bellman segment is absorbed automatically into the new initial conditions. Recomputing the optimal control problems with these new initial conditions compensates for all previous propagation errors, preventing them from being carried over to the remaining part of the computation, i.e., it prevents the accumulation of the interpolation and propagation errors.

VII. Results from the Bellman Pseudospectral Method

To successfully implement a Bellman PS method, the first thing that needs to be determined is the choice of Bellman segments. From the physics of the problem, it is clear that the accuracy of the first burn has the most effect on the final error. It suggests that the first Bellman segment should start right before the first burn. Furthermore, placing the Bellman segments right before the burn could take maximum advantage of the grid distribution of a PS method, i.e., high density around the two ends of the segments.

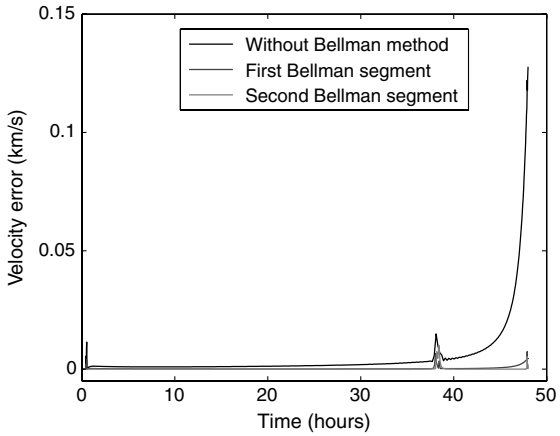

Fig. 14 Velocity error.

We solved the trajectory optimization problem on this new segment with 500 LGL nodes. Shown in Figs. 13 and 14 are the position and velocity errors. From these figures, we can see the position and velocity errors increase rapidly after the first burn without the Bellman PS method, and this trend is greatly restricted when we reoptimize the problem in the first Bellman segment, since there are more LGL points to capture the first burn to reduce the interpolation errors. By applying the Bellman technique just once, the terminal error has been reduced significantly; see Table 3. To further reduce the error to the desired accuracy of $\mathcal{O}(1\text{ km}, 1 \times 10^{-3}\text{ km/s})$, we choose the second Bellman segment starting after the first burn. The computation results shown in Figs. 13 and 14 demonstrate that two Bellman segments are sufficient to achieve the given high accuracy.

Table 3 compares the final position errors, velocity errors, and fuel consumption using the Bellman PS method with the ones using the standard PS method. The final position and velocity errors reduce to 24.56 km and 4.68×10^{-3} km/s from 643.95 km and 1.28×10^{-1} km/s. The fuel consumption is 6656.71 kg, compared with 6655.71 kg. Applying the Bellman PS method again at the end of the first burn, we find the interpolation error to be rejected almost completely, and the final position and velocity errors become 0.40 km and 2.06×10^{-5} km/s within the tolerance criterion. The fuel consumption is 6657.28 kg, which means a total of 1.58 kg fuel, or 0.02% more fuel, is used for the correction. The final, high-accuracy solutions are shown in the Figs. 15–17.

It is instructive to map the trajectory from Cartesian coordinates to osculating elements. Figure 18 shows the semimajor axis, eccentricity, and inclination time histories. From the Figs. 15–18, it is apparent that the first burn appears at the periapsis to raise apoapsis and change the circular parking orbit into a larger elliptic orbit ($e = 0.89$). The steering angle varies almost linearly with time. The angle between the thrust vector and velocity is about three degrees, indicating that the thrust is applied approximately along the tangential direction of the trajectory. The second burn is located near the apoapsis and the majority of the burn is used to change the inclination about from 105 to 90 deg, and the thrust vector points along an inertially fixed direction. That the optimal burn direction is inertially fixed to perform a plane change maneuver has been noted previously [38]. What is interesting about our solution is that the second burn that performs the plane change appears to be singular. The singular arc analysis on the thrust profile is further discussed in Park et al. [34,35]. The third burn takes place near the end of the flight time (48 hours), which places the spacecraft into a hyperbolic

Table 3 Effects of the Bellman PS method

Methods	Position error, km	Velocity error, km/s	Fuel consumption, kg
Standard PS	643.95	1.28e − 1	6655.71
First Bellman segment	24.56	4.68e − 3	6656.71
Second Bellman segment	0.40	2.06e − 5	6657.28

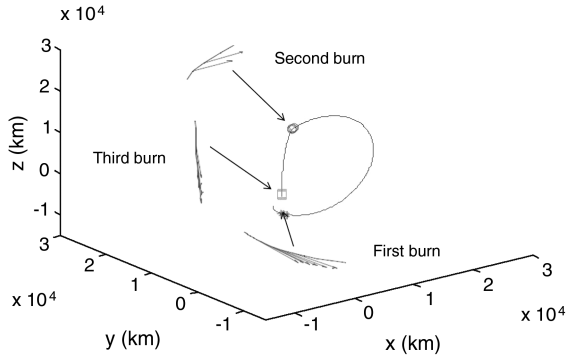

Fig. 15 Trajectory and burn position.

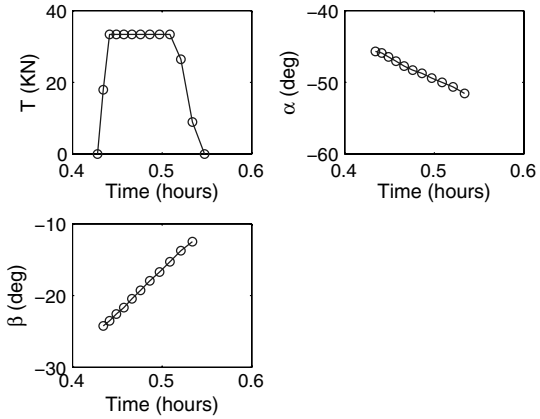

Fig. 16 First burn.

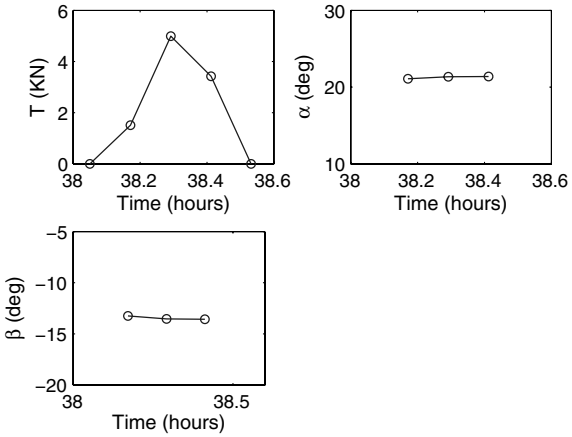

Fig. 17 Singular burn.

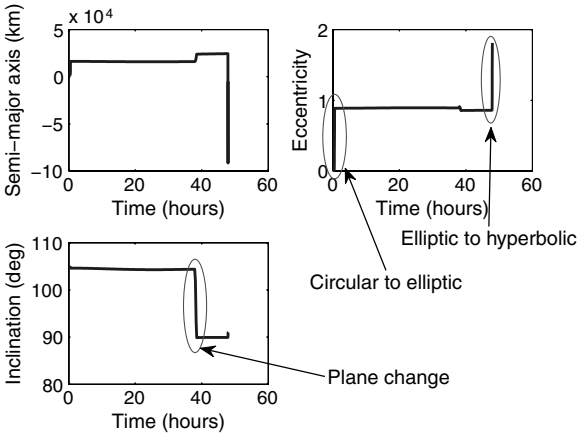

Fig. 18 Osculating elements.

trajectory. The direction of the burn varies smoothly with time. The angle between the thrust vector and velocity is about 12 deg, and the majority of the burn is used for increasing energy to escape the moon gravity field.

VIII. Conclusions

The Bellman PS method can be used to generate high-accuracy solutions for high-fidelity trajectory optimization problems. This technique successfully rejects the propagation error stemming from control implementation and results in a finite-thrust, high-accuracy optimal moon-Earth transfer trajectory. This implies that the proposed technique may be used to generate high-accuracy solutions for a manned lunar mission in a single simulation using the standard Legendre PS method. No assumptions need to be made on the thrust switching structure, and the procedure does not use a starting impulsive approximation. The optimality of the computed solution can be easily verified by a joint application of Pontryagin's principle and the covector mapping principle. Because the difference in fuel between the Bellman PS method and the standard PS method is negligible, the standard PS method may be used with confidence to accurately determine fuel requirements for mission analysis. In contrast, the Bellman PS method may be used to compute high-accuracy trajectories for practical implementation.

Acknowledgments

We gratefully acknowledge funding for this research provided in part by U.S. Naval Postgraduate School under Grant N00244-10-1-0049. We would like to thank one of the anonymous reviewers for independently validating our results.

References

[1] Miele, A., and Wang, T., "Near-Optimal Guidance Scheme for a Mars Trajectory," *Acta Astronautica*, Vol. 51, No. 1, 2002, pp. 351–378. doi:10.1016/S0094-5765(02)00039-5

[2] Weeks, M. W., Marchand, B. G., Smith, C. W., and Scarritt, S. K., "Design of the Onboard Autonomous Targeting Algorithm for the Trans-Earth Phase of Orion," *AIAA Guidance, Navigation, and Control Conference and Exhibit*, AIAA Paper 2008-7262, 2008.

[3] D'Souza, C., Crain, T., and Clark, F. C., "Orion Cislunar Guidance and Navigation," *AIAA Guidance, Navigation, and Control Conference and Exhibit*, AIAA Paper 2007-6681, 2007.

[4] Webb, E., "Three-Impulse Transfer from Lunar Orbits," *AAS Science and Technology Series*, Vol. 11, 1967, pp. 541–552.

[5] Edelbaum, T. N., "Optimal Nonplanar Escape from Circular Orbits," *AIAA Journal*, Vol. 9, No. 12, 1971, pp. 2432–2436. doi:10.2514/3.50047

[6] Williams, J., Davis, E. C., Lee, D., Condon, G. L., Dawn, T. F., and Qu, M., "Global Performance Characterization of the Three Burn Trans-Earth Injection Maneuver Sequence over the Lunar Nodal Cycle," *Advances in the Astronautical Sciences*, Vol. 135, Part 3, Univelt Publishers, San Diego, CA, 2010, pp. 1297–1316.

[7] Condon, G. L., Dawn, T. F., Merrian, R. S., Sostaric, R. R., and Westhelle, C. H., "CEV Trajectory Design Considerations for Lunar Missions," *Advances in the Astronautical Sciences*, Vol. 128, Univelt Publishers, San Diego, CA, 2007, pp. 663–682.

[8] Ocampo, C., and Saudemont, P. R., "Initial Trajectory Model for a Multi-Maneuver Moon to Earth Abort Sequence," *Journal of Guidance, Control, and Dynamics*, Vol. 33, No. 4, 2010, pp. 1184–1194. doi:10.2514/1.46955

[9] Ocampo, C., and Munoz, J. P., "Variational Equations for a Generalized Spacecraft Trajectory Model," *Journal of Guidance, Control, and Dynamics*, Vol. 33, No. 5, 2010, pp. 1615–1622. doi:10.2514/1.46953

[10] Scarritt, S. K., Marchand, B. G., and Weeks, M. W., "An Autonomous Onboard Targeting Algorithm Using Finite Thrust Maneuvers," *AIAA Guidance, Navigation, and Control Conference and Exhibit*, AIAA Paper 2009-6104, Chicago, IL, 2009.

[11] Ross, I. M., "A Beginner's Guide to DIDO: A Matlab Application Package for Solving Optimal Control Problems," Elissar Global, http://www.ElissarGlobal.com [retrieved March 2011], 2007.

[12] Bedrossian, N. S., Bhatt, S., Kang, W., and Ross, I. M., "Zero-Propellant Maneuver Guidance," *IEEE Control Systems Magazine*, Oct. 2009, pp. 53–73.

doi:10.1109/MCS.2009.934089
[13] Kang, W., and Bedrossian, N., "Pseudospectral Optimal Control Theory Makes Debut Flight, Saves NASA $1M in Under Three Hours," *SIAM News*, Vol. 40, No. 7, Sept. 2007, p. 1.
[14] Karpenko, M., Bedrossian, N., Bhatt, S., Fleming, A., and Ross, I. M., "First Flight Results on Time-Optimal Spacecraft Slews," *21st AAS/AIAA Spaceflight Mechanics Meeting*, AAS Paper 11-110, 2010.
[15] Keesey, L., "TRACE Spacecraft's New Slewing Procedure," *NASA Heliophysics Feature Stories*, Dec. 2010, http://www.nasa.gov/mission_pages/sunearth/news/trace-slew_prt.htm [retrieved March 2011].
[16] Riehl, J. P., Paris, S. W., and Sjauw, W. K., "Comparison of Implicit Integration Methods for Solving Aerospace Trajectory Optimization Problems," *AIAA/AAS Astrodynamics Specialist Conference and Exhibit*, AIAA Paper 2006-6033, 2006.
[17] Yan, H., Gong, Q., Park, C., Ross, I. M., and D'Souza, C. N., "High Accuracy Moon-Earth Escape Trajectory Optimization," *AIAA Guidance, Navigation, and Control Conference and Exhibit*, AIAA Paper 2010-7726, Aug. 2010.
[18] Park, C., Gong, Q., Ross, I. M., and Sehkavat, P., "Fuel-Optimal Design of Moon-Earth Trajectories Using Legendre Pseudospectral Method," *AIAA/AAS Astrodynamics Specialist Conference and Exhibit*, AIAA Paper 2008-7074, 2008.
[19] Elnagar, G., Kazemi, M. A., and Razzaghi, M., "The Pseudospectral Legendre Method for Discretizing Optimal Control Problems," *IEEE Transactions on Automatic Control*, Vol. 40, No. 10, 1995, pp. 1793–1796.
doi:10.1109/9.467672
[20] Fahroo, F., and Ross, I. M., "Costate Estimation by a Legendre Pseudospectral Method," *Journal of Guidance, Control, and Dynamics*, Vol. 24, No. 2, 2001, pp. 270–277.
doi:10.2514/2.4709
[21] Gong, Q., R. I. M., and Fahroo, F., "Costate Computation by a Chebyshev Pseudospectral Method," *Journal of Guidance, Control, and Dynamics*, Vol. 33, No. 2, 2010, pp. 623–628.
doi:10.2514/1.45154
[22] Fahroo, F., and Ross, I. M., "Advances in Pseudospectral Methods for Optimal Control," *AIAA Guidance, Navigation, and Control Conference and Exhibit*, AIAA Paper 2008-7309, Honolulu, HI, 2008.
[23] Fahroo, F., and Ross, I. M., "Pseudospectral Methods for Infinite-Horizon Optimal Control Problems," *Journal of Guidance, Control, and Dynamics*, Vol. 31, No. 4, 2008, pp. 927–936.
doi:10.2514/1.33117
[24] Williams, P., "Jacobi Pseudospectral Method for Solving Optimal Control Problems," *Journal of Guidance, Control, and Dynamics*, Vol. 27, No. 2, 2004, pp. 293–297.
doi:10.2514/1.4063
[25] Ross, I. M., and Fahroo, F., "Pseudospectral Knotting Methods for Solving Optimal Control Problems," *Journal of Guidance, Control, and Dynamics*, Vol. 27, No. 3, 2004, pp. 397–405.
doi:10.2514/1.3426
[26] Fahroo, F., and Ross, I. M., "Convergence of the Costates Does Not Imply Convergence of the Control," *Journal of Guidance, Control, and Dynamics*, Vol. 31, No. 5, 2008, pp. 1492–1497.
doi:10.2514/1.37331
[27] Ross, I. M., and Gong, Q., "Emerging Principles in Fast Trajectory Optimization," Elissar Global, Monterey, CA, 2010, http://www.ElissarGlobal.com [retrieved March 2011].
[28] Gong, Q., Kang, W., and Ross, I. M., "A Pseudospectral Method for the Optimal Control of Constrained Feed-back Linearizable Systems," *IEEE Transactions on Automatic Control*, Vol. 51, No. 7, 2006, pp. 1115–1129.
doi:10.1109/TAC.2006.878570
[29] Gong, Q., Ross, I. M., Kang, W., and Fahroo, F., "Connections between the Covector Mapping Theorem and Convergence of Pseudospectral Methods for Optimal Control," *Computational Optimization and Applications*, Vol. 41, No. 3, 2007, pp. 307–335.
doi:10.1007/s10589-007-9102-4
[30] Kang, W., "The Rate of Convergence for a Pseudospectral Optimal Control Method," *47th IEEE Conference on Decision and Control*, IEEE Publications, Piscataway, NJ, 2008, pp. 521–527.
[31] Gong, Q., Fahroo, F., and Ross, I. M., "A Spectral Algorithm for Pseudospectral Methods in Optimal Control," *Journal of Guidance, Control, and Dynamics*, Vol. 31, No. 3, 2008, pp. 460–471.
doi:10.2514/1.32908
[32] Polak, E., *Optimization: Algorithms and Consistent Approximations*, Springler–Verlag, Heidelberg, 1997.
[33] Ross, I. M., *A Primer on Pontryagin's Principle in Optimal Control*, Collegiate Publishers, San Francisco, CA, 2009.
[34] Park, C., Yan, H., Gong, Q., and Ross, I. M., "Numerical Verification of Singular Arcs from Moon to Earth Transfer," *Advances in the Astronautical Sciences*, Vol. 136, Part 1, 2010, pp. 73–88.
[35] Park, C., Ross, I. M., Yan, H., and Gong, Q., "Necessary Conditions for Singular Arcs Involving Multiple Gravitational Bodies," *Advances in the Astronautical Sciences*, Vol. 136, Part 1, 2010, pp. 107–122.
[36] Ross, I. M., Gong, Q., and Sekhavat, P., "Low-Thrust High-Accuracy Trajectory Optimization," *Journal of Guidance, Control, and Dynamics*, Vol. 30, No. 4, 2007, pp. 921–933.
doi:10.2514/1.23181
[37] Ross, I. M., Gong, Q., and Sekhavat, P., "The Bellman Pseudospectral Method," *AIAA/AAS Astrodynamics Specialist Conference and Exhibit*, AIAA Paper 2008-6448, 2008.
[38] Zondervan, K. P., Wood, L. J., and Caughey, T. K., "Optimal Low-Thrust, Three-Burn Orbit Transfers with Large Plane Changes," *The Journal of the Astronautical Sciences*, Vol. 32, No. 3, 1984, pp. 407–427.